Research

Check for updates

Authors for correspondence:
David Correa
e-mail: david.correa@uwaterloo.ca
Simon Poppinga
e-mail: simon.poppinga@biologie.
uni-freiburg.de

[†]These authors contributed equally to this study.

4D pine scale: biomimetic 4D printed autonomous scale and flap structures capable of multi-phase movement

David Correa[1,2,†], Simon Poppinga[3,4,†],
Max D. Mylo[3,5], Anna S. Westermeier[3],
Bernd Bruchmann[6], Achim Menges[1] and
Thomas Speck[3,4,5]

[1]Institute for Computational Design and Construction (ICD), University of Stuttgart, Stuttgart, Germany
[2]School of Architecture, University of Waterloo, Cambridge, Ontario, Canada
[3]Plant Biomechanics Group, Botanic Garden, [4]Freiburg Materials Research Center (FMF), and [5]Cluster of Excellence livMatS, University of Freiburg, Freiburg im Breisgau, Germany
[6]BASF SE Advanced Materials and Systems Research, Ludwigshafen, Germany

DC, 0000-0002-4399-7897; SP, 0000-0001-5341-9188;
MDM, 0000-0001-5744-9069; ASW, 0000-0001-9281-1254;
AM, 0000-0001-9055-4039; TS, 0000-0002-2245-2636

We developed biomimetic hygro-responsive composite polymer scales inspired by the reversible shape-changes of Bhutan pine (*Pinus wallichiana*) cone seed scales. The synthetic kinematic response is made possible through novel four-dimensional (4D) printing techniques with anisotropic material use, namely copolymers with embedded cellulose fibrils and ABS polymer. Multi-phase motion like the subsequent transversal and longitudinal bending deformation during desiccation of a natural pinecone scale can be structurally programmed into such printed hygromorphs. Both the natural concept generator (Bhutan pinecone scale) and the biomimetic technical structure (4D printed scale) were comparatively investigated as to

their displacement and strain over time via three-dimensional digital image correlation methods. Our bioinspired prototypes can be the basis for tailored autonomous and self-sufficient flap and scale structures performing complex consecutive motions for technical applications, e.g. in architecture and soft robotics.

This article is part of the theme issue 'Bioinspired materials and surfaces for green science and technology (part 3)'.

1. Introduction

(a) Motivation

Motile plant structures (e.g. petals, leaves) represent efficient and functionally robust compliant mechanisms [1]. They perform aesthetic shape-changes without nerves, muscles and discrete hinges and are increasingly recognized as suitable concept generators for the development of biomimetic shape-changing structures [2–5]. Four-dimensional (4D) printing of such devices has become an emerging field [6–10], but the movement patterns of the bioinspired structures realized so far are limited in terms of temporal and spatial versatility and programmability. On the contrary, nature holds ready a multitude of plant movement actuation and deformation principles and consecutive motion patterns [11–14]. Understanding the respective form–structure–function relationships of the biological concept generators and implementing the motion principles at work into technical devices would open a versatile toolbox for generating biomimetic structures with tailored motion responses. These could have various applications ranging from micro-electromechanics, microfluidics, soft robotics to architecture. In this study, we aimed at abstracting the complex multi-phase movement of Bhutan pinecones and to achieve similar modes of actuation and deformation in 4D printed structures, which can serve as a basis for the development of versatile and self-sufficient scale and flap systems.

(b) Biological concept generators of the biomimetic approach

Our biological concept generators are cone seed scales of the Bhutan pine (*Pinus wallichiana* Jacks., Pinaceae). In general, pinecones are well known to be in a closed state under wet environmental conditions (keeping the seeds safe and avoiding release of the airborne seeds) and to open when it is dry (releasing the seeds for dispersal mainly by wind; figure 1*a,b*) [15]. Such passive water-driven motion responses are nastic and, therefore, structurally 'programmed' into the individual seed scales. Each scale forms a functional bilayer structure through a gradation in its tissue structure, from the sclereid cells at the bottom of the scale to a region of sclerenchymatous strands at the top (figure 1*c–l*). Whereas the sclereid layer is the actuating (active) layer, the sclerenchymatous layer is the resistance (passive) layer. Both layers together dictate an upward scale bending upon water uptake and differential swelling (wet environment, the cone closes) and a downward bending upon desiccation (dry environment, the cone opens) [15,17–19]. Bending is restricted to a short zone at the basal part of the scale [19]. The moving pinecone scales are able to generate considerable blocking forces of around 3 N [20]. Furthermore, the structural integrity of the cone scales can be conserved for millions of years, highlighting extraordinary functional resilience and robustness [21].

The stratification of the pinecone scale's functional bilayer set-up is not homogeneous and the dimensions of sclereid and sclerenchymatous tissues vary over the length of the individual scale (figure 1*c–f*). The sclerenchyma forms cable-like structures, which extend into the scale periphery, where they are inserted into the apophysis (figure 1*d–h*). There is no tight 'bonding' between the actuating sclereid and resistive sclerenchyma layers, as the sclerenchymatous strands are embedded into a rather soft matrix of 'brown tissue' (*sensu* [15,17–22]) and can often be easily torn apart from the sclereid layer by hand (figure 1*d–k*). In addition, the degree of lignification is
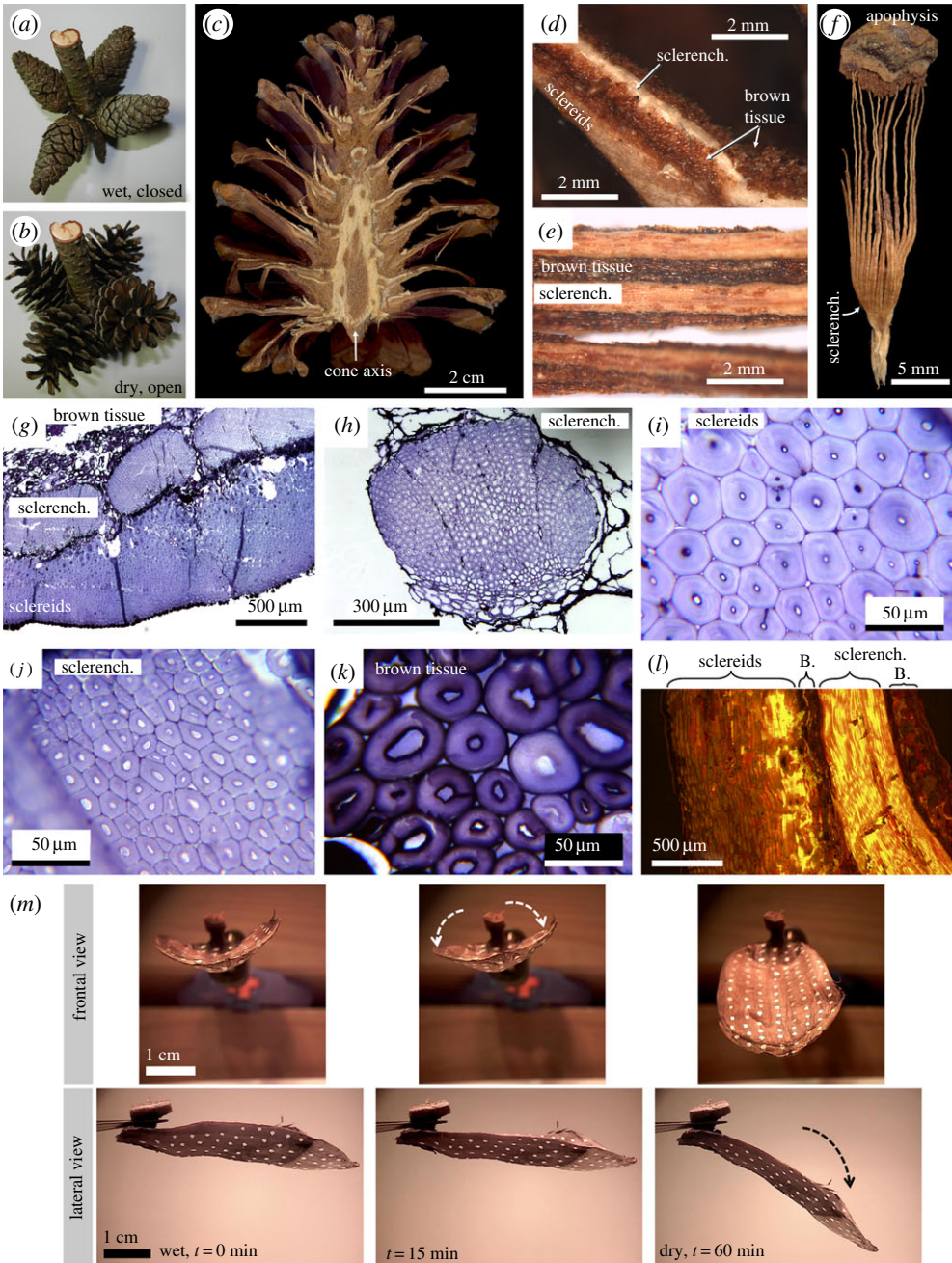
Figure 1. (Caption overleaf.)

not clearly delimited between the lower actuating and upper resistive layer, with the sclereid layer showing increasing degrees of lignification towards the highly lignified sclerenchyma (figure 1l). In summary, the structural set-up of pinecone seed scales is very complex and variable among the individual scales and not yet fully understood in respect to the characteristics of the individual hygroscopic bending deformation.

In preliminary investigations, we found that the seed scale of Bhutan pine performs a bi-axial two-phase hygroscopic movement [16] (figure 1m). When the scale is wet, it is almost straight (without any conspicuous longitudinal curvature), but it possesses a notable transversal curvature at its apical part, with the margins being curved upwards. During desiccation, this

Figure 1. (*Overleaf.*) Pinecone seed scale functional morphology and kinematics. The scales passively react to changing environmental humidity conditions leading to a closed cone when it is wet (*a*) and to an open cone when it is dry (*b*). A longitudinally halved cone in the dry condition (*c*). The actuating sclereid layer is not tightly connected to the sclerenchymatous strands, which are embedded in a matrix of 'brown tissue' (*sensu* [15]) (*d,e*) and reach towards the apical apophysis (*f*). Images (*d–f*) modified from [16]. Light microscopy image of a semi-thin cross section of the functional bilayer set-up (*g*), one sclerenchymatous strand (*h*), a detail of the sclereid layer (*i*), a detail of the sclerenchymatous strand (*j*), and a detail of the 'brown tissue' (*k*). Fluorescence microscopy of an acridine orange-stained semi-thin longitudinal section of a scale (*l*). The brightness indicates degree of lignification, which is of increasing intensity in the sclereid layer towards the sclerenchymatous layer, high in the sclerenchymatous strand itself, and low in the 'brown tissue' (abbreviated as 'B.'). (*m*) The bi-axial, two-phase, passive-nastic movement of the Bhutan pine (*Pinus wallichiana*) seed cone scale. An initially wet seed scale (in frontal and lateral view, clamped with its basal part by a forceps) undergoes two successive bending deformation processes upon desiccation (at approx. 20°C, approx. 50% RH). At the beginning ($t = 0$) the scale is wet, straight (without any conspicuous longitudinal curvature) and possesses a notable transversal curvature by which longitudinal bending is hindered. After $t = 15$ min, the transversal curvature alone has markedly decreased. Afterwards, the scale starts to bend longitudinally until a maximum bending angle (which depends on the extent of scale desiccation, i.e. on the environmental conditions) is achieved after $t = 60$ min. (Online version in colour.)

transversal curvature gradually decreases and the scale flattens without notable alterations of its longitudinal curvature. Afterwards, the scale bends longitudinally until it achieves a maximum bending angle. The functional bilayer set-up of the natural scale was the template for our 4D printed hygroscopic scale-like structures, where passive hydraulic actuation drives the tailored multi-phase bending deformation. For a better understanding of the complex movement behaviour, we performed three-dimensional (3D) deformation measurements on the natural and on the bioinspired printed scales' surfaces.

2. Material and methods

(a) Materialization and four-dimensional printing

3D printing through Fused Filament Fabrication (FFF) was applied, which works by the precise deposition of extruded molten thermoplastic polymer. The process of extrusion affects the microstructure of the polymer through the 'alignment of the polymer molecules along the axis of deposition' [23] and the shear-induced alignment of any fillers within the polymer [24–26]. This unique capacity to affect the material at that scale through the controlled fabrication process has been implemented into high-performance lightweight composites [27], nanofibre-reinforced polymers [28] and wood flour composites [29]. This inherent material capacity is instrumental in the design, control and manipulation of the hydration-mediated expansion of the responsive 3D printed layer [30].

Inspired by the pinecone, we used two materials with substantial performance differences, hygroscopic swelling characteristics, to transfer the resistance and actuation layer of the biological concept generator to form bilayer architectures. (1) The first material is a Wood Polymer Composite (WPC) composed of fibrous filler from wood-derived fibres (40%) combined with a co-polyester polymer matrix, as indicated by the manufacturer. The WPC mimics the properties of the swellable lower sclereid layer, i.e. the hygroscopically actuating layer of the natural pinecone seed scale. The WPC FFF 3D printing material was selected for this investigation based on the researchers' background experience with the material [6,30] and its readily commercial availability. (2) The second material is Acrylonitrile Butadiene Styrene (ABS), which is a common 3D printing polymer that does not contain fibrous fillers. ABS is susceptible to moisture, which affects its mechanical performance [31] and printing quality [32], but it undergoes negligible dimensional changes compared to WPC [33]. ABS acts as the stiffer and much lesser swellable upper layer, made of sclerenchymatous strands in the real cone scale, also considered as the

resistance layer. An initial test sample was created using thermoplastic polyurethane (TPU) as it bonds better during the 3D printing process, however, while the TPU polymer has better adhesion properties to the WPC material it is also more susceptible to elongation [34] and therefore it was not used in subsequent tests. This material architecture forms the basis for design methodologies that can define the localized shape-change curvature.

All composite samples had a nominal dimension of 45×100 mm in length and were printed using a 0.25 mm vertical layer height, with a total of four layers for all samples, on a flat heated bed on air. After printing, all samples were laminar and had no curvature in either longitudinal or axial directions. All samples were printed using the commercially available Laywood, WPC filament (CC Products) and ABS filament (Makerbot). Both filaments were prepared for printing by reducing their moisture contents using a dehumidification chamber at 70°C for 24 h and were stored in a controlled environment prior to print.

The print paths were generated using discreet tool path geometries modelled in a Computer-Aided Design platform (Houdini 14) via a python script and then transferred to the 4D printer (Makerbot Replicator 2X) via the slicer software (Makerbot desktop) using their native binary X3G file format. Samples were printed using a 0.4 mm brass nozzle (220°C) directly on the heated print bed (60°C) covered on a single layer of standard masking tape. After the print was complete, the samples were allowed to cool on the bed before being removed.

Photographic images were taken with a DSLR camera and full format mirrorless digital cameras (Sony A7S and Nikon D7100) with both a 28 mm and a 35 mm lens using time intervals between 45 and 60 s. Continuous lighting of the samples was provided via metal halide and LED photography lamps.

The synthetic scale underwent a moisture-induced deformation from flat state (right after print) to a positive doubly curved shape state. Under desorption, the scale underwent continuous shape-change deformation from the positive Gaussian curvature, to flat and then into a new negative Gaussian curvature. The experimental set-up consisted of a cycle of moisture absorption by the specimen using direct immersion in water followed by a desorption cycle via a drying oven (40°C). Some initial tests included image registration at ambient conditions (at RT, RH ∼ 20%). Both of these set-ups were practical to test the shape-change deformation from full saturation (after immersion) to desiccation. However, this set-up did not provide sufficient control to correlate specific shape configurations to specific relative humidity and temperature parameters. It is speculated that a climate-controlled chamber could be used to precisely identify the relative humidity and temperature required to allow the scale to return to a flat state without going into negative curvature.

(b) Kinematical and three-dimensional deformation analyses

We recorded the desiccation-induced motion (at RT, RH ∼ 60%) of an initially wet Bhutan pinecone seed scale simultaneously from lateral and frontal view with two USB microscopes (Conrad, Hirschau, Germany) to gain initial qualitative information on its deformation during movement. The wet scales were taken from a water basin and recorded immediately.

For quantitatively analysing kinematics and motion repeatability, we recorded a Bhutan pinecone seed scale and a 4D printed scale (which is capable of the two-phase motion sequence, see results) from lateral positions with one of the above-mentioned USB cameras. Before the individual recordings, the scales were each fixed with clamps for stability and immersed in water for at least 4 h to ensure complete wetting. Afterwards, they were transferred into a drying oven (40°C) and the desiccation movement was recorded (experiment starts with first movement sequence). Afterwards, the scales were transferred into a water-filled aquarium and the motions recorded (second movement sequence). The desiccation- and swelling-induced movements were repeated multiple times and the angular changes (deg) over time (min) were analysed with Fiji/ImageJ [35]. The experiments included idle periods in the oven or in the aquarium overnight and/or over weekends.

Displacement and strain during the desiccation-driven motions of the initially fully wetted natural and printed scales were analysed in detail using a stereo-camera set-up and the software GOM Aramis Professional (Professional 2016, GOM GmbH, Braunschweig, Germany). Time-lapse recordings were performed on a granite table in a chamber with constant environmental conditions (23°C, RH 36%) at the Plant Biomechanics Group, Freiburg University. Two USB-3 cameras (PL D685CU, pixel size 4.8 μm) and the Capture OEM software (v. 2.3.7.9) (both by PixeLINK, Rochester, New York, USA) were used. Each camera was mounted on a micro-manipulating device placed on a rail (custom-made by the technical workshop, Institute for Biology II/III, University of Freiburg, Germany) and equipped with a 50 mm lens (Planar T* 1,4/50, Carl Zeiss AG, Oberkochen, Germany) by using mount adapters (NIK-C, Kipon, Shanghai, China). A distance between both camera sensors of about 24 cm and a distance between their midpoints and the specimen of about 52 cm was installed, resulting in a stereo angle of approx. 26°. A cold light source (Techno Light 270, Karl Storz GmbH & Co. KG, Tuttlingen, Germany) was used for illumination. Calibration was performed with a target grid panel (CP 20, GOM GmbH, Braunschweig, Germany; thermal expansion coefficient: $4.00*10^{-6}\,K^{-1}$; certification temperature: 20°C). Scale surface contrast was enhanced by applying a stochastic speckle pattern using black spray paint (Professional, Liquitex, Cincinnati, Ohio, USA). For the biological pine scale an additional white priming (Premium Weißlack Seidenmatt, Peter Kwasny GmbH, Gundelsheim, Germany) was applied. In summary, we analysed five natural and three printed scales with very similar resulting deformation and strain patterns, and one representative each was chosen for presentation in this article.

Images were captured every 10 min and 20 min during desiccation of the biological and 4D printed scales, respectively. The resulting recording times were 1360 min for the natural scale and 1760 min for the printed scale, as presented here. In the case of the natural scale, the lower side with the actuating layer was recorded, and in the case of the artificial scale, its upper side (where both actuating and resistance layers are visible). Stereo image stacks were analysed using the digital image correlation-based (3D-DIC) GOM Aramis software. Facet sizes of 24 pixels and 32 pixels and maximal point distances of 8 pixels and 16 pixels were chosen as correlation parameters for the biological and the 4D printed scales, respectively. Three-dimensional displacement and (Cauchy) strain values parallel to the scales apex-base connection and parallel to the largest lateral dimensions were calculated in reference to the fully wet state.

(c) Histological analyses

Depicting the anatomical complexity of pinecone seed scales (figure 1) required histological examinations. Natural pinecone seed scales were embedded and cut as semi-thin cross or longitudinal sections after a protocol published in [36]. We applied either toluidine-blue staining (infiltration for 2 min in toluidine C.I. 52040, 1 min washing with de-ionized water), or acridine-orange staining after a protocol published in [37]. Pictures were taken with an Olympus BX61 light microscope and an Olympus DP71 camera (Olympus Europa, Hamburg, Germany) using the software Cell^P 2.8 (Olympus Soft Imaging Solutions, Münster, Germany).

3. Results

(a) 4D printing of a functional model inspired by the Bhutan pinecone

A functional model of the bi-axial curvature deformation was initially printed using an oriented TPU layer (one layer 0.25 mm thick) in combination with discreet WPC regions for each axis (one layer 0.25 mm thick), longitudinal (dominant) and transverse directions (figure 2). TPU and WPC can bond to each other easily during printing so that very simple bilayer structures can be created. For this test, each raster pattern, longitudinal and transversal, was oriented perpendicular to the desired axis of bending to form a directed bilayer region. That is, each layer had an anisotropic material orientation directly perpendicular to each other. This model was useful for identifying
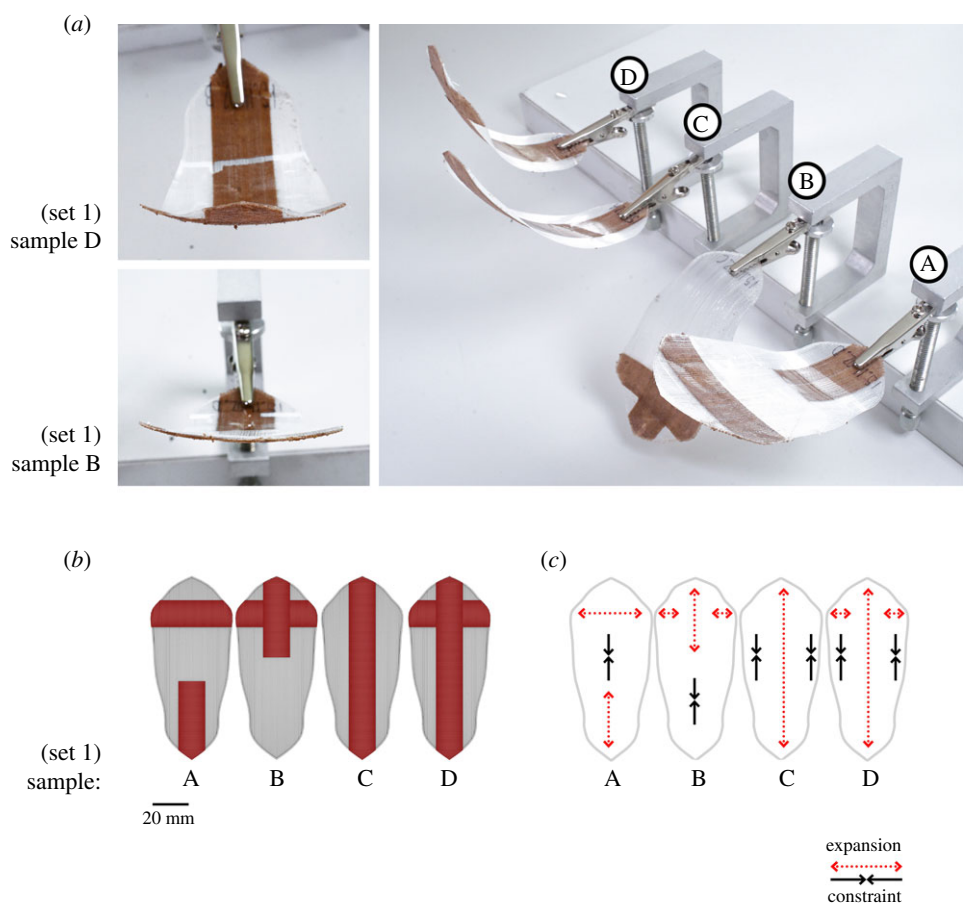
Figure 2. The 4D functional model of the bi-axial curvature deformation. An initial set of 3D printed scales using differentiated bilayer regions composed of a constraint layer of oriented TPU and an oriented hygroscopic layer of WPC. (*a*) Fully wet 4D printed samples show different double curvature deformations in response to localized bilayer structure. (*b*) Localized WPC raster pattern regions in relation to global shape of scale. (*c*) The direction of hygroscopically induced expansion on WPC layer shown in relation to dominant axis of oriented TPU constraint. (Online version in colour.)

the differentiated curvature regions found in the basal and apical region. The 4D printed model could reach both target curvatures for the dry and wet states of the pine scale but this model failed to achieve the two-stage kinematic response motion that the natural scale performs (figures 1*m* and 2). It is speculated that, while the oriented TPU layer physically connects the two functional regions within the scale, a negligible amount of stress is transferred from one region to the other. In this case, each region's shape deformation takes place simultaneously but independently from each other and therefore results in a single-stage actuation movement.

Then, a different bilayer architecture was developed that integrated longitudinal ABS filament strings similar to the sclerenchymatous strands as present in the natural scale. Unlike the previous curvature model, the bilayer was not formed by two discrete overlapping layers but incorporated a more complex inter-layer connection, referred to here as a 'weave' architecture that mechanically fastened both materials (figures 3–8). This set-up was inspired by the graded functional bilayer set-up of natural pinecone seed scales, as described in the Introduction (figure 1*c–l*). In this model, the continuous longitudinal ABS strips were interwoven with an upper and lower WPC raster pattern over two different layers with a 1:1 ratio of transverse to longitudinal print paths (figure 3). Similar to the natural scale, the abstracted model relied on the creation of a material matrix where the primary non-expanding ABS constraints are enclosed between the upper and lower raster layers, probably preventing delamination (figure 1*d,e,i*). Following the same
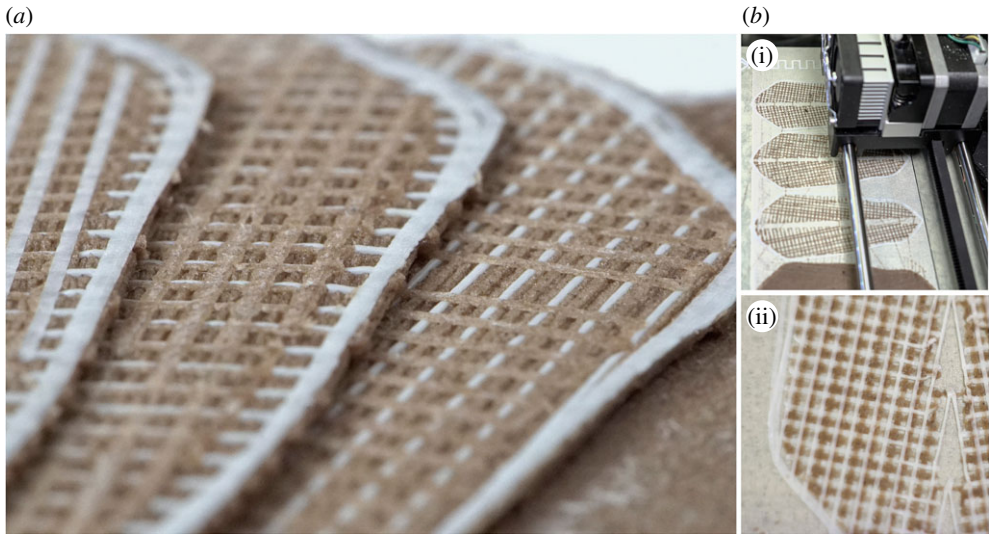
Figure 3. 3D printing multi-material process to create the 4D printed artificial pine scales. Several different raster patterns were produced using ABS and WPC to test and evaluate suitable bilayer architectures. (*a*) After printing, all samples are laminar and have no curvature in either longitudinal or axial directions. (*b*) Photo of 3D printing process exposing 'weave' architecture at multiple states of print completion. (Online version in colour.)

approach as the sclerenchymatous strands, the ABS strings (cables) were fused to the boundary constraint at both the basal and apical endpoints (figure 1*f*). The resulting global shape changes can be seen in figures 4–8. It has to be noted that the printed samples went from flat (after printing) to having bi-axial curvature when wet (positive curvature) to then also bi-axial curvature when desiccated (negative curvature), which might have been a temperature-dependent effect.

To understand the interrelation between the 'cables' and the oriented hygroscopic layers, a total of 24 test samples were printed. In sets of four pieces, each set used a different variation on the hygroscopic WPC grain pattern. Three WPC grain orientations were tested (0°, 10° and 80°). As the sclerenchymatous strands in the pinecone scale follow a mirrored symmetry orientation along the transversal axis (cf. [17]), originating from the basal region, the same strategy was used for the samples at 10° and 80° (figures 5 and 7). Within the set of four, one sample was printed having only the longitudinal constraint cables, the second sample contained only cross-sectional constraints, the third sample contained both longitudinal cables with cross-sectional constraints; the fourth sample was printed as a control without cables or cross-sectional constraints. To test the influence of the anatomical edge of the pine scale, an additional duplicate set was printed for each that also includes an outer periphery boundary constraint. Sample 'A' with bidirectional constraints presented the desired two-stage actuation observed in the pine scale (figures 7 and 8; electronic supplementary material, movie S1).

(b) Kinematics and three-dimensional deformation analyses of natural and four-dimensional printed cone scales

In total, we recorded 54 successive movement sequences of a Bhutan pinecone scale (alternatingly driven by desiccation in a drying oven, and by swelling under water in an aquarium; electronic supplementary material, figure S1a). During the swelling movements, angular changes of $23.4 \pm 5.5°$ ($n = 27$) were reached after 55 min. During the slower desiccation-driven movements, angular changes of $22.7° \pm 4.8°$ ($n = 27$) were reached after 115 min. After the complete 54 motion cycles, the scale appeared as structurally undamaged from the outside, with no visible delamination effects.
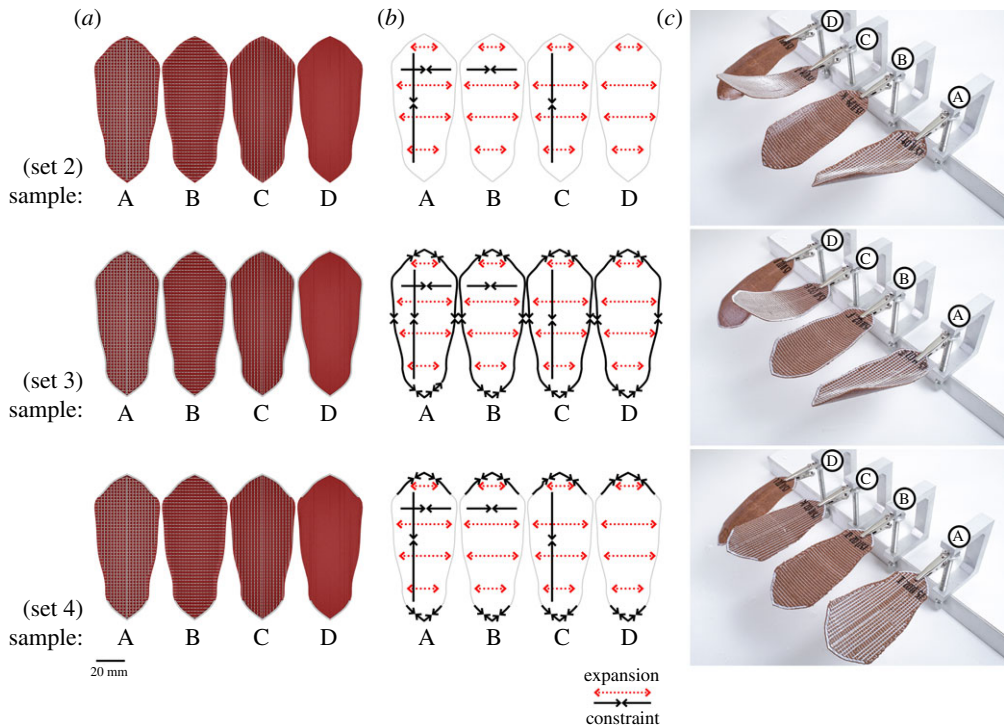
Figure 4. 4D printed scales with a 'weave' bilayer architecture and with WPC raster pattern at 0° from the scale's longitudinal axis. Having the same 3D printed raster pattern for all three sets of samples (*a*), 4D scales show different shape deformations when fully wet (*c*) in response to changes to the bilayer constraints in both the longitudinal and lateral axis as well as the boundary edge of the scale (*b*). Samples with single constraints in either longitudinal or lateral directions (sets 2–4, B and C samples) had simple bending deformation perpendicular to the constraint direction, consistent with simple bilayer behaviour. Samples with constraints in both axes (sets 2–4, A samples) had a twist bending deformation. Samples with no axial constraints presented very limited shape change (sets 2–4, D samples). (Online version in colour.)

The displacement and strain analyses on the natural Bhutan pinecone scale (figure 9*a–c*) corroborate our preliminary qualitative observations of the natural multi-phase motion (figure 1*m*). In a first motion step, synchronous displacement of the apical lateral 'flaps' of the scale leads to a 'flattening' of the scale (the transversal curvature decreases). Then the scale starts to bend longitudinally, leading to the fully bent scale at the end of the desiccation-driven process ($t = 1000$ min). We find a gradual increase of displacement along the longitudinal scale axis with the apical part (the scale tip) moving the most (1.8 cm max. displacement), whereas the basal part (which is naturally attached to the cone axis) does not move at all (figure 9*a*). The measured strong negative strain (up to 6% shrinkage) in *x*-direction (along the longitudinal scale axis, see coordinates in figure 9*b*) occurs mainly at the basal part of the scale, where it becomes more and more prominent over the measured timescale (figure 9*b*). By contrast, the strong negative strain in *y*-direction (up to 5% shrinkage) along the transverse axis of the scale (figure 9*c*) becomes increasingly prominent and distributed along the lateral parts of the scale. In summary, we find two co-occurring deformation behaviours on the actuating lower side of the Bhutan pinecone scale, which are opposite in direction.

Similar to our analysis of the Bhutan pinecone seed scale movement, we recorded 13 successive movements alternatingly driven by desiccation and swelling of a 4D printed scale (electronic supplementary material, figure S1*b*). During the desiccation movements, angular changes of $17.1° \pm 1.4°$ ($n = 7$) were reached after 190 min. During the slower swelling movements, angular changes of $15.5° \pm 0.5°$ ($n = 6$) were reached after 390 min. After the complete 13 motions, the
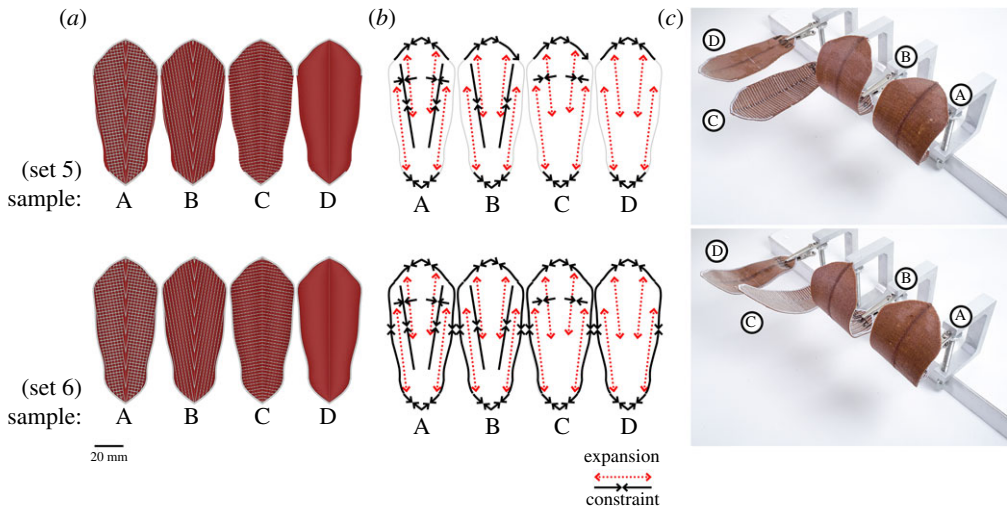
Figure 5. 4D printed scales with 'weave' bilayer architecture and oriented 80° symmetrically mirrored WPC raster pattern. Using the same 3D printed raster pattern for both sets of samples (*a*), 4D scales show different shape deformations when fully wet (*c*) in response to changes to the bilayer constraints in both the longitudinal and lateral axis as well as the boundary edge of the scale (*b*). The high aspect ratio of the pine scale also has an impact on the amount of displacement that can be observed between different regions of the scale. When the primary axis of deformation is perpendicular to the longitudinal axis (longer axis) a higher level of displacement can be seen between the basal and the apical region. Therefore, having the WPC and the constraints oriented almost perpendicular to the longitudinal axis allowed for the bending deformation to occur over the longest length of the scale, resulting in a larger deformation with smaller curvature radius (sets 5 and 6, samples A and B) (*c*). The additional lateral or boundary constraints in the A samples do not appear to have any significant impact in the shape deformation (*c*) while a significant longitudinal bending change can be observed between the C samples of both sets 3 and 4 as a result of the boundary constraint. Both C samples have lateral constraints that are parallel to the raster pattern and direction of expansion, which results in limited bending, so the addition of the longitudinal boundary constraint results in a noticeable change in bending radius between set 5 and 4. Since the objective is to achieve the pine scale's bi-axial two-stage motion, as per $1.2 (cf. figure 1*m*), the consistent single-axis curvature change across the entire scale, achieved by samples A and B (for both sets), is not suitable for the required performance goals. (Online version in colour.)

3D printed scale appeared as structurally damaged from the outside, with visible delamination effects.

The 4D printed scale exhibits a very similar two-phase motion behaviour as the natural scale (figures 1*m* and 9*d–f*), by first showing displacement of the apical, lateral flaps (flattening) which is then followed by pronounced longitudinal bending of the whole scale (figure 9*d*). However, the strain fields are different to those we found in the natural scale, as no such distinct, co-occurring and opposing deformation domains can be detected. Moderate negative strain in *x*-direction (along the longitudinal scale axis, figure 9*e*) occurs distributed all over the scale over all measured time-points, with several irregularly dispersed, strongly affected 'islands'. By contrast, strong negative strain in *y*-direction (along the transverse axis of the scale, figure 9*f*) was detected mainly on the middle and outer parts of the scale, where only a little ABS plastic was printed.

4. Discussion

Biomimetic transfer and implementation of plant movement principles can lead to technical structures with completely new functionalities, like micro-lenses with snap-buckling induced focal point tuning [38] or jumping microgels [39]. The natural pinecone seed scale is a functionally very reliable structure capable of repeated motion sequences, which makes it an excellent model
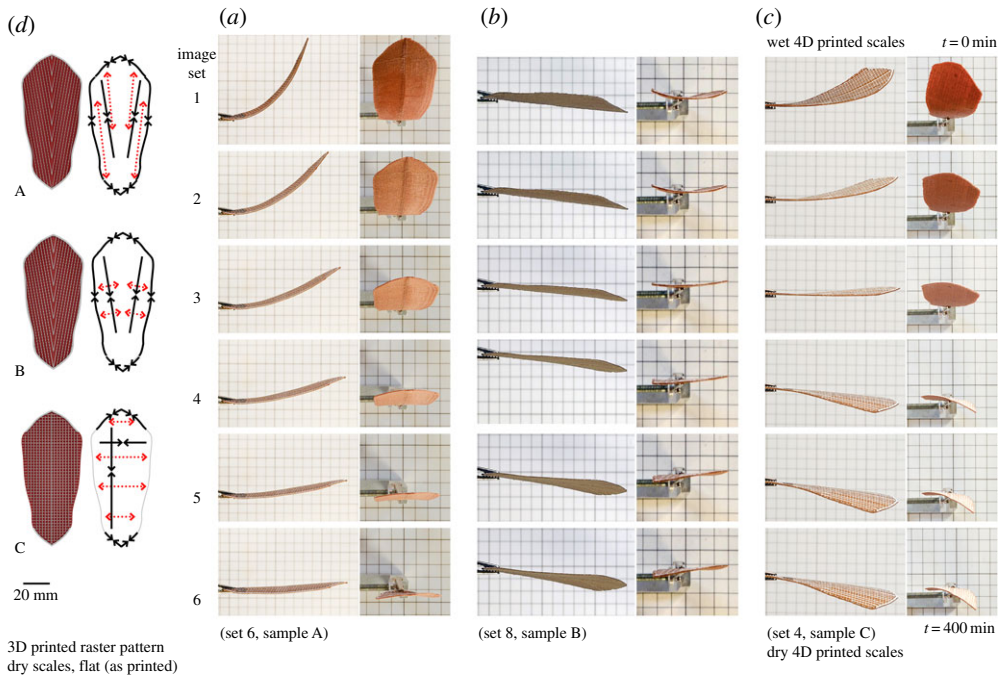
Figure 6. The 4D printed artificial scale's distinct shape bending deformation, of three different bilayer architectures A, B and C (d), upon desiccation. All three scales are clamped at the basal region and present a continuous, single-phase, actuation bending of predominantly single-axis curvature change. Each sample demonstrates a differentiated shape-change deformation based on the bilayer architecture (d). Starting fully wet (t = 0, image set 1), sample A (a) presents notable longitudinal curvature with negligible transversal curvature, sample B (b) presents the opposite condition with notable transversal curvature with negligible longitudinal curvature, sample C (c) presents curvature change at an approximate 45° from the longitudinal axis, resulting in a twist. All samples demonstrate a single actuation stage (image sets 1–6) with a continues curvature change along a single primary axis: sample A (a) presents continues curvature change along longitudinal axis, sample B (b) along the transversal axis while sample's C (c) deformation may be described as a continuous bidirectional 'twist' deformation. Since the objective is to achieve the pine scale's bi-axial two-stage motion, as per $1.2 (cf. figure 1m), the consistent single-axis curvature change across the entire scale, achieved by these three samples (A–C), is not suitable for the required performance goals. (Online version in colour.)

for studying natural compliant mechanisms for biomimetics. We successfully transferred a two-step multi-phase motion sequence observed in Bhutan pinecone scales into a 4D printed artificial scale. Our investigations regarding such 'design spaces' for continuous and successive kinematics constitute a very promising aspect for future studies, where the individual motions steps could be triggered (or actuated) by various means, e.g. changes in environmental conditions like humidity [40], temperature [41], pH [42] or light [43].

Aside from the technical aspect and merit of our biomimetic approach, we describe a previously unknown two-phase motion sequence in natural *P. wallichiana* cone seed scales. Apart from mere bending motions as described for other *Pinus* species (e.g. [15,17,18]), the movement observed here (during desiccation) is more complex and starts with a transversal curvature change, which is then followed by longitudinal curvature change. Probably, the pronounced transversal curvature in the wet state (corresponding to the closed cone when all scales are bent upwards) causes a higher flexural stiffness, leading to a better mechanical protection from seed predation (cf. [44]), hinders longitudinal bending by increasing the moment of inertia, and probably leads to an improved 'packing' of scales. By contrast, the more flat configuration allows for the longitudinal bending deformation allowing for cone opening and seed release. Preliminary, unpublished analyses revealed very similar multi-phase motion behaviour in cone
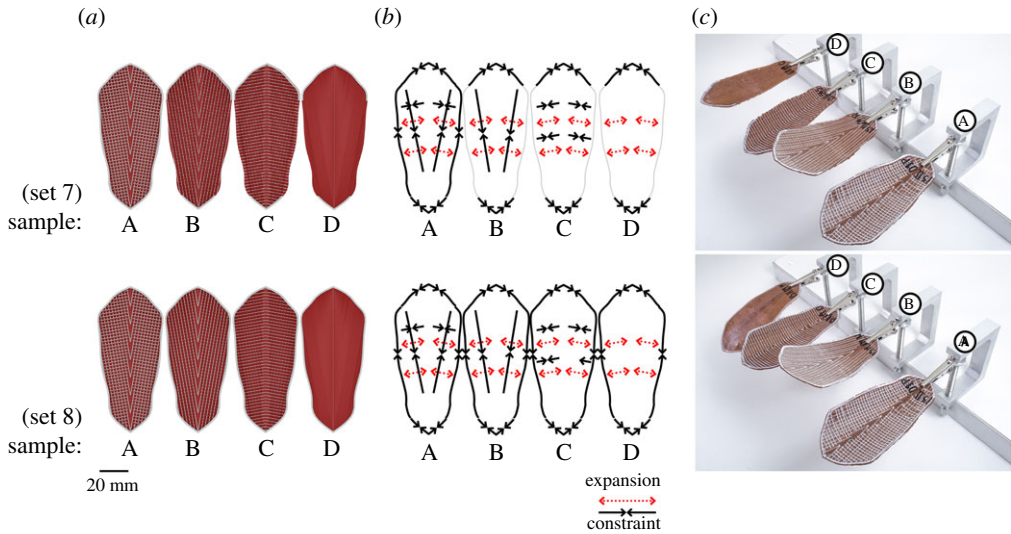
Figure 7. 4D printed scales with 'weave' bilayer architecture and oriented 10° symmetrically mirrored WPC raster pattern. Using the same 3D printed raster pattern for both sets of samples (*a*), 4D scales show different shape deformations when fully wet (*c*) in response to changes to the bilayer constraints in both the longitudinal and lateral axis as well as the boundary edge of the scale (*b*). Having the WPC and the constraints oriented almost parallel to the longitudinal axis limits the bending deformation as the primary bending axis occurs over a shorter lateral direction. However, the change in angle from 0° to 10° combined with the mirrored symmetry of the raster pattern provides two longer and differentiated bending axis near the apical region. Samples with longitudinal or lateral constrains showed doubly curved shape deformation with a very small amount of two-stage actuation while sample 'A' with bidirectional constraints (same specimen for both sets) presented the desired two-stage actuation observed in the pine scale. Subsequent tests indicated that since the longitudinal constraints and the boundary had identical orientation there was not observable difference in the shape-changing behaviour between a continuous and a discontinuous boundary constraint in this case. (Online version in colour.)

scales of Sugar pine (*P. lambertiana*), and it remains to be investigated which other species possess similar kinematics and how and why they have evolved. In a recent study [45], the interrelation of longitudinal and transverse curvature changes in *P. pinaster* cone scales, the environmental humidity regime and the scale shape and thickness has been quantitatively described, which further helps our understanding of complex shape changes in such natural actuators.

Regarding the observed deformation as measured in the natural scale, we assume that the pronounced negative strain in *x*-direction (figure 9*b*) at the scale base dictates the longitudinal bending of the whole scale (leading to cone opening), whereas the laterally pronounced negative strain in *y*-direction is responsible for the 'flattening' of the scale, which is initially (in the wet state) strongly curved transversally. Although the motion pattern of the artificial 4D printed scale is similar to that of the natural one, the measured strain fields (figure 9*e,f*) are different to some extent in comparison to those of the natural scale. We hypothesize that the observed moderate negative strain in *x*-direction on more or less the whole scale dictates the longitudinal bending, whereas the negative strain in *y*-direction on the middle and lateral parts of the scale dictates the change in transversal curvature (displacement of lateral flaps). As the ABS strands on the scale surface are aligned in *y*-direction, only in the regions where no ABS strands have been printed (in the middle and very lateral parts) can negative *y*-strain occur.

It has to be noted that the duration for the full desiccation movements of the natural and printed scales as measured during the deformation and strain analyses (figure 9) is much longer than those measured during the preliminary recording (figure 1*m*) and during the movement
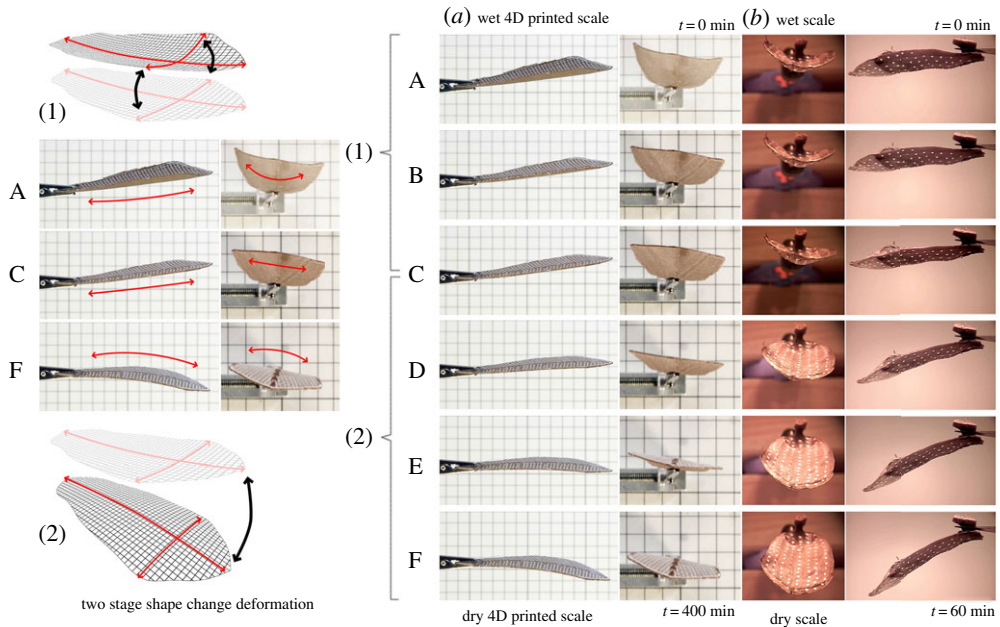
Figure 8. 4D printed artificial scale two-phase shape deformation (*a*) compared with two-phase passive-nastic movement of the Bhutan pine scale (*b*). Both scales are clamped at the basal region and undergo two successive bending deformations upon desiccation. The two separate sequences indicate a different image registration timescale, highly variable due to environmental conditions, and therefore, comparative image sets were created to match the deformation stages as opposed to the time. Starting fully wet ($t = 0$, image set A) both scales present notable transversal curvature with negligible longitudinal curvature. At the first actuation stage (image sets A–C), transversal curvature alone has markedly decreased. This first stage is then followed by a significant change in longitudinal curvature until a maximum bending angle is reached (image sets C–F). (Online version in colour.)

repeatability tests (electronic supplementary material, figure S1). This is because the application of the stochastic speckle pattern by using black spray paint slows down evaporation of water from these scales. However, because the spray coating is very thin, we assume that it only affects evaporation (and, thereby, movement speed), but not the process of movement itself, which is structurally predetermined. Interestingly, the 4D printing scale tested during the movement repeatability investigations (electronic supplementary material, figure S1) showed a faster desiccation movement response than during swelling, presumably due to internal hygroscopic stresses that arise during variation of moisture content (cf. ref. [46]). This is in contrast to our tests with the natural cone scale, where swelling (water uptake during full immersion in water) is faster than desiccation (evaporation of water out of the scale). However, we may speculate that evaporation of water out of the sprayed-up cellulose fibrils is somehow enhanced (e.g. due to heating up by photography lights) and/or that a certain amount of water has to be taken up by the scale first for movement induction, which might explain this observation.

Our movement repeatability investigations (electronic supplementary material, figure S1) show that natural scales of Bhutan pine are functionally very resilient by being capable of more than 50 successive full motion sequences, which is presumably way beyond their 'biological purpose'. The scale's structural integrity is maintained during the testing cycles and no apparent delamination of the different tissues occurs. This corroborates earlier investigations [21], assuming a high functional and structural robustness of conifer cones by showing that even millions of years old, fossilized cone scales are still capable of hygroscopic movements. Our 4DP scale in contrast still lacks such robustness, as it showed signs of delamination after
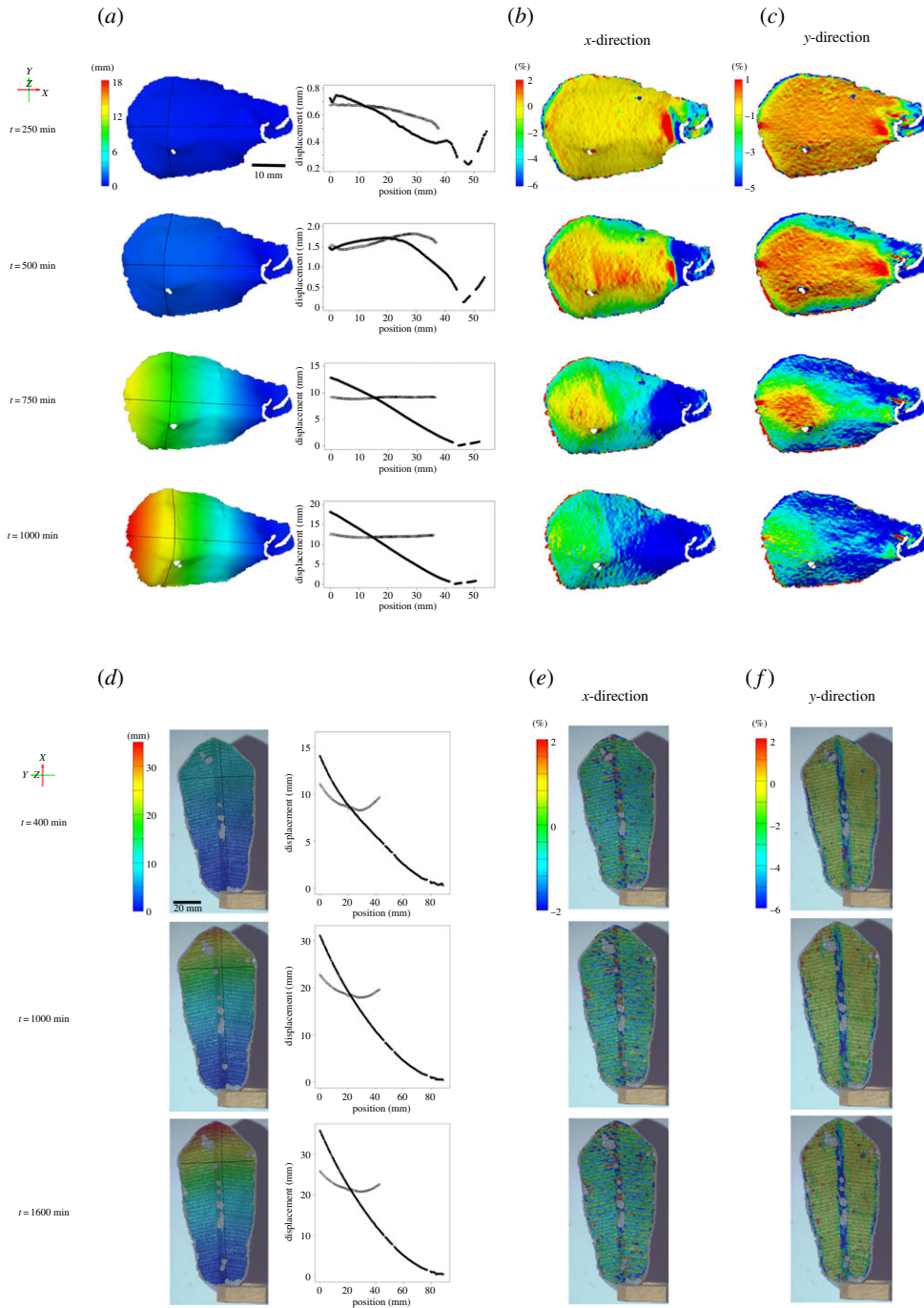
Figure 9. (*Caption overleaf.*)

13 movements. Deterioration in the reversibility of the material is consistent with previous investigations on WCP bilayers [8] where it is speculated that 'mechanosorptive degradation' might affect the wood–polymer interface. Future studies should tackle such issues, also with regard to the development of weather-resistant anti-fouling materials for architectural outdoor applications [47].

Figure 9. (*Overleaf.*) Displacement and strain measurements on the natural Bhutan pinecone scale and on the 4D printed artificial scale. The lower side of the pinecone scale (where the actuating layer is situated) was recorded during desiccation and analysed (*a–c*). For the printed scale, the upper side of the scale (where the actuating and resistance layer can be seen) was recorded during desiccation and analysed (*d–f*). The coordinates and timescale (min) are indicated, as well as colour schemes for displacement (mm) and strain ((%), *x*- and *y*-direction) values. The graphs, which correspond to the displacement analysis, show the displacement values of every point on the analysed longitudinal line (pinecone scale: from left, apical, to right, basal position; printed scale: from top, apical, to down, basal position) (filled circles) and on the transverse line (empty circles) after the indicated timescale. (*a*) It can be seen that, first, a displacement of the lateral flaps of the scale occurs, leading to the observed 'flattening'. In the end, at $t = 1000$ min, the scale has completely bent and a gradual increase of displacement can be clearly seen along the longitudinal axis of the scale, with the basal part (which is naturally connected to the cone axis) not having moved at all (blue colour) and the apical part having moved the most (red colour). An increasingly prominent and strong negative strain (shrinkage) in *x*-direction (*b*) occurs over the observed timescale on the basal part of the scale, whereas a strong negative strain in *y*-direction (*c*) is distributed to a greater extent on the scale incorporating also the lateral flaps. Note that the overall scale motion here takes longer than the one in the preliminary experiment (figure 1*m*). This is because the application of the stochastic speckle pattern by using black spray paint, as required for the applied DIC analyses (see Methods section), slows down evaporation of water from these scales. (*d*) Similar to in the natural scale, it can be seen that in the printed scale, first, the displacement of the lateral flaps of the scale occurs. In the end, at $t = 1600$ min, the scale has completely bent. A striking negative strain (shrinkage) in *x*-direction (*e*) occurs over almost the whole scale surface, whereas strong strain in *y*-direction (*f*) was only detected on the middle and very lateral parts of the scale, where only little ABS plastic as resistance layer was printed. (Online version in colour.)

5. Conclusion

Our study can act as inspiration for future approaches where on-demand kinetic structures with tailored movement responses are required. The unique contribution of our bioinspired 4D printing method lies in the ability to define local hygroscopic anisotropies and local non-hygroscopic anatomic features in a single process using readily available materials by using bioinspired material strategies from the pinecone scale. The study also highlights the role that state-of-the-art testing methodologies can play in validating bioinspired models and analysing the complex behaviour of bioinspired composite 4D printing structures with differentiated functional regions. As promising prospects, it can be postulated that more complex three-dimensional architectures could be analysed and tested via 4D printing, and that there is generally great potential to achieve multi stage complex actuation movement by applying abstract models of bioinspired plant movement and material organization strategies. For architectural applications, these novel multi-stage actuation movements can lead the way to develop advanced and passively actuated façade systems, with highly tailored shape-change capacity. It is a very promising prospect for future biological studies to investigate the interrelation of scale architecture (cellular characteristics at different regions) in combination with the scale biomechanics (e.g. by AFM measurements) and the locally successive evaporation of water (probably via MRI) [48,49], altogether leading to the observed multi-phase motion. Our analyses show the potential of full-field 3D displacement and deformation analyses for evaluation and validation of movement principles in plants and technical structures.

References

1. Poppinga S, Körner A, Sachse R, Born L, Westermeier AS, Hesse L, Knippers J, Bischoff M, Gresser GT, Speck T. 2016 Compliant mechanisms in plants and architecture. In *Biomimetic research for architecture and building construction: biological design and integrative structures. Biologically-inspired systems* (eds J Knippers, T Speck, K Nickel), pp. 169–193. Berlin, Germany: Springer.
2. Guo Q, Dai E, Han X, Xie S, Chao E, Chen Z. 2015 Fast nastic motion of plants and bioinspired structures. *J. R. Soc. Interface* **12**, 20150598. (doi:10.1098/rsif.2015.0598)
3. Schleicher S, Lienhard J, Poppinga S, Speck T, Knippers J. 2015 A methodology for transferring principles of plant movements to elastic systems in architecture. *Comput. Aided Des.* **60**, 105–117. (doi:10.1016/j.cad.2014.01.005)
4. Li S, Wang KW. 2017 Plant-inspired adaptive structures and materials for morphing and actuation: a review. *Bioinsp. Biomim.* **12**, 011001. (doi:10.1088/1748-3190/12/1/011001)
5. Speck T, Bauer G, Masselter T, Poppinga S, Schmier S, Thielen M, Speck O. 2018 Biomechanics and functional morphology of plants - inspiration for biomimetic materials and structures. In: *Plant biomechanics* (eds A Geitmann, J Gril), pp. 399–422. Berlin, Germany: Springer.
6. Correa D, Papadopoulou A, Guberan C, Jhaveri N, Reichert S, Menges A, Tibbits S. 2015 3D-printed wood. Programming hygroscopic material transformations. *3D Print. Addit. Manuf.* **2**, 106–116. (doi:10.1089/3dp.2015.0022)
7. Gladman AS, Matsumoto EA, Nuzzo RG, Mahadevan L, Lewis JA. 2016 Biomimetic 4D printing. *Nat. Mater.* **15**, 413–419. (doi:10.1038/nmat4544)
8. Le Duigou A, Castro M, Bevan R, Martin N. 2016 3D printing of wood fibre biocomposites: from mechanical to actuation functionality. *Mater. Design* **96**, 106–114. (doi:10.1016/j.matdes.2016.02.018)
9. Ding Z, Yuan C, Peng X, Wang T, Jerry Qi H, Dunn ML. 2017 Direct 4D printing via active composite materials. *Sci. Adv.* **3**, e1602890. (doi:10.1126/sciadv.1602890)
10. Arslan H, Nojoomi A, Jeon J, Yum K. 2018 3D printing of anisotropic hydrogels with bioinspired motion. *Adv. Sci.* **6**, 1800703. (doi:10.1002/advs.201800703)
11. Burgert I, Fratzl P. 2009 Actuation systems in plants as prototypes for bioinspired devices. *Phil. Trans. R. Soc. A* **367**, 1541–1557. (doi:10.1098/rsta.2009.0003)
12. Poppinga S, Masselter T, Speck T. 2013 Faster than their prey: new insights into the rapid movements of active carnivorous plants traps. *Bioessays* **35**, 649–657. (doi:10.1002/bies.201200175)
13. Charpentier V, Hannequart P, Adriaenssens S, Baverel O, Viglino E, Eisenman S. 2017 Kinematic amplification strategies in plants and engineering. *Smart Mater. Struct.* **26**, 063002. (doi:10.1088/1361-665X/aa640f)
14. Knippers J, Schmid U, Speck T. (eds). 2019 *Biomimetics for architecture: learning from nature*. Basel, Switzerland: Birkhäuser.
15. Shaw GRS. 1914 *The genus pinus.* Publications of the Arnold Arboretum No. 5. Rolling Meadows: The Riverside Press.
16. Poppinga S, Speck T. 2015 New insights into the passive nastic motions of pine cone scales and false indusia in ferns. In Proc. of the 8th Plant Biomechanics Int. Conf., Nagoya, Japan.

17. Harlow WM, Cote WA, Day AC. 1964 The opening mechanism of pinecone scales. *J. For.* **62**, 538–540. (doi:10.1093/jof/62.8.538)

18. Dawson C, Vincent JFV, Rocca A-M. 1997 How pinecones open. *Nature* **390**, 668. (doi:10.1038/37745)

19. Reyssat E, Mahadevan L. 2009 Hygromorphs: from pine cones to biomimetic bilayers. *J. R. Soc. Interface* **6**, 951–957. (doi:10.1098/rsif.2009.0184)

20. Le Duigou A, Castro M. 2016 Evaluation of force generation mechanisms in natural, passive hydraulic actuators. *Sci. Rep.* **6**, 18105. (doi:10.1038/srep18105)

21. Poppinga S, Nestle N, Šandor A, Reible B, Masselter T, Bruchmann B, Speck T. 2017 Hygroscopic motions of fossil conifer cones. *Sci. Rep.* **7**, 40302. (doi:10.1038/srep40302)

22. Le Duigou A, Beaugrand J, Castro M. 2017 Compréhension des mécanismes d'actionneurdes pommes de pin pour améliorer les performances des biocomposites hygromorphes. *Journées Nationales sur les Composites*, École des Ponts ParisTech (ENPC), Jun 2017, 77455 Champs-sur-Marne, France. hal-01623672.

23. Cole DP, Riddick JC, Iftekhar JHM, Strawhecker KE, Zander NE. 2016 Interfacial mechanical behavior of 3D printed ABS. *J. Appl. Polym. Sci.* **133**, 43671. (doi:10.1002/app.43671)

24. Bell JP. 1969 Flow orientation of short fiber composites. *J. Compos. Mater.* **3**, 244–253. (doi:10.1177/002199836900300204)

25. Murty KN, Modlen GF. 1977 Experimental characterization of the alignment of short fibers during flow. *Polym. Eng. Sci.* **17**, 848–853. (doi:10.1002/pen.760171207)

26. Langhans K, Roeder E. 1992 Theoretische und experimentelle Untersuchungen zur Faserausrichtung beim Strangpressen von Kurzfaser-Verbundwerkstoffen. *Materialwiss. Werkst.* **23**, 174–179. (doi:10.1002/mawe.19920230509)

27. Compton BG, Lewis JA. 2014 4D-printing of lightweight cellular composites. *Adv. Mater.* **26**, 5930–5935. (doi:10.1002/adma.201401804)

28. Shofner ML, Lozano K, Rodríguez-Macías FJ, Barrera EV. 2003 Nanofiber-reinforced polymers prepared by fused deposition modeling. *J. Appl. Polym. Sci.* **89**, 3081–3090. (doi:10.1002/app.12496)

29. Pitt K, Lopez-Botello O, Lafferty AD, Todd I, Mumtaz K. 2017 Investigation into the material properties of wooden composite structures with in-situ fibre reinforcement using additive manufacturing. *Compos. Sci. Technol.* **138**, 32–39. (doi:10.1016/j.compscitech.2016.11.008)

30. Correa D, Menges A. 2015 3D printed hygroscopic programmable material systems. *MRS Proc.* **1800**, 1016. (doi:10.1557/opl.2015.644)

31. Kim E, Shin Y-J, Ahn S-H. 2016 The effects of moisture and temperature on the mechanical properties of additive manufacturing components: fused deposition modeling. *Rapid Prototyp. J.* **22**, 887–894. (doi:10.1108/RPJ-08-2015-0095)

32. Månsson A. 2017 How moist filaments will screw up your 3D-printing. See https://3dprinterchat.com/2016/12/how-moist-filaments-will-screw-up-your-3d-printing/, last accessed on 23.10.2018.

33. Kariz M, Sernek M, Kuzman M. 2018 Effect of humidity on 3D-printed specimens from wood-pla filaments. *Wood Res.* **63**, 917–922.

34. Gelhausen MG, Feuerbach T, Schubert A, Agar DW. 2018 3D printing for chemical process laboratories I: materials and connection principles. *Chem. Eng. Technol.* **41**, 618–627. (doi:10.1002/ceat.201700294)

35. Schindelin J *et al.* 2012 Fiji: an open-source platform for biological-image analysis. *Nat. Methods* **9**, 676–682. (doi:10.1038/nmeth.2019)

36. Bunk K, Fink S, Speck T, Masselter T. 2017 Branching morphology, vascular bundle arrangement and ontogenetic development in leaf insertion zones and ramifications of three arborescent Araliaceae species. *Trees* **31**, 1793–1809. (doi:10.1007/s00468-017-1585-8)

37. Bohn HF, Günther F, Fink S, Speck T. 2015 A passionate free climber: structural development and functional morphology of the adhesive tendrils in *Passiflora discophora*. *Int. J. Plant Sci.* **176**, 294–305. (doi:10.1086/680231)

38. Holmes DP, Crosby AJ. 2007 Snapping surfaces. *Adv. Mat.* **19**, 3589–3593. (doi:10.1002/adma.200700584)

39. Lee H, Xia C, Fang NX. 2010 First jump of microgel; actuation speed enhancement by elastic instability. *Soft Matter* **6**, 4342–4345. (doi:10.1039/C0SM00092B)

40. Zhang L, Liang H, Jacob J, Naumov P. 2015 Photogated humidity-driven motility. *Nat. Commun.* **6**, 7429. (doi:10.1038/ncomms8429)

41. Jiang S, Liu F, Lerch A, Ioniv L, Agarwal S. 2015 Unusual and superfast temperature-triggered actuators. *Adv. Mat.* **27**, 4865–4870. (doi:10.1002/adma.201502133)

42. Lin Q, Li L, Tang M, Hou X, Ke C. 2018 Rapid macroscale shape morphing of 3D-printed polyrotaxane monoliths amplified from pH-controlled nanoscale ring motions. *J. Mater. Chem. C* **6**, 11956. (doi:10.1039/C8TC02834F)

43. Iamsaard S, Aßhoff SJ, Matt B, Kudernac T, Cornelissen JJ, Fletcher SP, Katsonis N. 2014 Conversion of light into macroscopic helical motion. *Nat. Chem.* **6**, 229–235. (doi:10.1038/nchem.1859)

44. Elliott PF. 1974 Evolutionary responses of plants to seed-eaters: Pine squirrel predation on Lodgepole pine. *Evolution* **28**, 221–231. (doi:10.2307/2407323)

45. Lin S, Xie YM, Li Q, Huang X, Zhou S. 2016 On the shape transformation of cone scales. *Soft Matter* **12**, 9797. (doi:10.1039/c6sm01805j)

46. Le Duigou A, Requil S, Beaugrand J, Scarpa F, Castro M. 2017 Natural fibres actuators for smart bio-inspired hygromorph biocomposites. *Smart Mater. Struct.* **26**, 125009. (doi:10.1088/1361-665X/aa9410)

47. Poppinga S, Zollfrank C, Prucker O, Rühe J, Menges A, Cheng T, Speck T. 2018 Toward a new generation of smart biomimetic actuators for architecture. *Adv. Mat.* **30**(Special Issue: Bioinspired Materials), 1703653. (doi:10.1002/adma.201703653)

48. Hesse L, Bunk K, Leupold J, Speck T, Masselter T. 2019 Structural and functional imaging of large and opaque plant specimen. *J. Exp. Bot.* **70**, 3659–3678. (doi:10.1093/jxb/erz186)

49. Hesse L, Leupold J, Poppinga S, Markus W, Strobel K, Masselter T, Speck T. 2019 Resolving form–structure–function relationships in plants with MRI for biomimetic transfer. *Integr. Comp. Biol.* **59**, 1713–1726. (doi:10.1093/icb/icz051)